ELSEVIER

Experimental Thermal and Fluid Science 26 (2002) 473–485

Experimental Thermal and Fluid Science

www.elsevier.com/locate/etfs

A condensation heat transfer correlation for millimeter-scale tubing with flow regime transition

Wei-Wen William Wang [1], Thomas D. Radcliff *, Richard N. Christensen

Department of Mechanical Engineering, The Ohio State University, Columbus, OH 43210, USA

Received 30 June 2000; received in revised form 15 December 2001; accepted 7 February 2002

Abstract

This study documents local convection heat transfer and flow regime measurements for HFC-134a condensing inside a horizontal rectangular multi-port aluminum condenser tube of 1.46 mm hydraulic diameter. The data is compared with condensation heat transfer correlations and flow regime maps from the literature. Existing correlations are found to overpredict both heat transfer and the stratified-to-annular flow regime transition velocity. Results of the experiments suggest that liquid drawn into the corners of the tube alter the phase distribution in the annular flow regime as well as stabilizing the annular flow regime at lower vapor velocities. To predict the heat transfer data, two correlations, each representing the physics of the specific phase distributions, are developed. A boundary layer analysis is applied for annular flow, in which the friction multiplier and dimensionless boundary layer temperature are evaluated specifically for this tube configuration. For stratified flow, documented film condensation and single-phase forced convection correlations are combined with straightforward void fraction weighting. Finally, a weighting correlation is successfully proposed to account for the all data regardless of the mix of flow regimes experienced. This weighting applies the result of a modified flow regime map developed from the flow visualizations. The final result is a practical correlation for the design of a condenser with millimeter-scale tubes.

Keywords: Condensation; Heat transfer; Flow regime; Microtube

1. Introduction

The use of millimeter-scale tubes for practical heat exchangers is made feasible by recent developments in aluminum extrusion and brazing processes. Typical tubes produced by this technology have parallel rectangular ports with hydraulic diameters on the order of 1 mm; much smaller than tubing traditionally used in heat exchangers. Compared with typical round-tube plate-fin condensers, these "minitube" condensers are more compact and lighter in weight for a given heat transfer capacity, and are thus of significant interest to industry.

The purpose of this research is to measure condensation heat transfer and visualize flow regime in a millimeter-scale tube, and then develop a correlation for the condensation heat transfer that accounts for changes in the phase distribution that can result because of the small, rectangular cross-section of the tube.

Correlations available to evaluate condensation heat transfer, as well as maps to predict flow regime, were developed from data for larger diameter tubes. For most correlations a single flow regime was assumed to dominate, although multiple flow regimes exist in real condensers. Surface tension effects in small diameter ducts can alter the conditions at which flow regime transitions occur, as well as the configuration of the phases in each specific regime. For these reasons, existing correlations and regime maps do not give consistent results at small diameters over a range of mass flux and quality.

Because practical millimeter-scale tube manufacturing technology is a recent development, few studies on these tubes have been published. The integral performance of minitube condensers is discussed by Goodremote et al. [1], Struss et al. [2], Struss and Gabbey [3], Sugihara and Lukas [4], and Tait et al. [5]. Major

* Corresponding author. Present address: Department of Mechanical Engineering, United Technologies Research Center, University of Akron, 411 Silver Lane, MS 129-19, East Hartford, CT 06108, USA. Tel.: +1-860-610-7514; fax: +1-860-610-2108.

E-mail address: radclitd@utrc.utc.com (T.D. Radcliff).

[1] Present address: Hydro Aluminum Adrian, Adrian, Michigan.

0894-1777/02/$ - see front matter
PII: S0894-1777(02)00162-0

Nomenclature

A	area
C_p	constant pressure specific heat
D_h	hydraulic diameter
e	energy balance index
f	flow regime fractional length
F	correction factor for crossflow heat exchanger
Fr_{so}	Soliman modified Froude number
G	mass flux
g	gravitational acceleration
h	heat transfer coefficient
i	enthalpy
j_v^*	superficial velocity
k	thermal conductivity
m	mass flow rate
Nu	Nusselt number
P	pressure
Pr	Prandtl number
Q	heat transfer rate
q	heat flux
R	thermal resistance
Re	Reynolds number
T	temperature
T_δ^+	dimensionless temperature difference across the liquid film
u_τ	$\sqrt{g\tau_w/\rho_l}$
U	overall heat transfer coefficient
x	quality
X_{tt}	turbulent–turbulent Lockhart Martinelli parameter
y^+	wall coordinate in the y-direction

Greek

α	void fraction
α	thermal diffusivity
δ	liquid film thickness
ε	turbulent thermal diffusivity
ϕ	two-phase pressure drop multiplier
η	efficiency
μ	viscosity
ρ	density
σ	shear stress
ν	kinematic viscosity

Subscripts

a	air
anul	annular flow
d	downstream
eq	equivalent
f	fluid
fg	latent
h	thermal
h	heater
i	inlet
l	liquid
l	lost
o	outlet
r	refrigerant
sat	saturation
strat	stratified flow
tot	total
trans	transitional
u	upstream
v	vapor
w	wall

improvements include reduced system charge, system miniaturization, and better heat transfer performance.

Several studies address condensation heat transfer in micro- and mini-tubes. Yang and Webb [6,7] utilized an R12-to-H_2O counterflow facility to examine plain and microfinned tubes with four parallel rectangular ports and hydraulic diameters of 2.637 and 1.564 mm, respectively. For condensation heat transfer they noted that the Akers and Rosson [8] correlation represented their experiments well, especially at lower mass flux, while other correlations tended to overpredict the Nusselt number. This correlation is based on an equivalent Reynolds number for the two-phase mixture developed to preserve interfacial shear in an annular flow.

Yang and Webb [9] then developed a semi-empirical model, based on Akers formulation, for heat transfer in finned microtubes. Separate models that account for the effects of vapor shear and surface tension were asymptotically combined into a single correlation. Although they had data for an HFC-134a condensation experiment that included 10-port plain tubing with a hydraulic diameter of 1.33 mm, a comparison to the new model was not given because they had achieved acceptable results using the Akers correlation without additional surface tension effects.

Moser et al. [10] subsequently noted that the formulation of Akers was flawed. In particular, they applied an analogy of heat and momentum transfer to determine that maintaining wall shear stress, rather than interfacial shear stress, is the appropriate basis for evaluating the equivalent Reynolds number. To predict the condensation coefficient using the equivalent Reynolds number of Moser et al., the frictional pressure gradient for the two-phase flow is required. Zhang [11] combined the model of Moser et al., with the pressure gradient predicted by the Friedel [12] correlation and found that the model

overpredicted the condensation coefficient of flat minichannel tubing by 20–50%, similar to existing correlations other than Akers'. Webb [13] recently suggested that the Friedel correlation does not accurately predict the R134a pressure gradient at saturation for tubing diameters below 2.13 mm. He presents a new correlation for the two-phase friction multiplier, developed by Zhang, based solely on quality and reduced pressure. This correlation, combined with the model of Moser et al., is stated to be capable of predicting condensation heat transfer coefficient in plain and finned tubes down to an equivalent diameter of 1.33 mm.

Real condensers, but not necessarily condenser experiments, will experience a range of flow regimes. The regimes experienced, and their transition points, depend on several parameters including inlet quality, pressure, tube diameter, and the local heat transfer coefficient. The equivalent Reynolds number formulation does not explicitly account for the effects of flow regime transition, nor do the friction factor models of Friedel and Zhang. This can be important when significant condensation occurs, as the same Re_{eq} can describe flows with single or multiple flow regimes. Dobson and Chato [14] visualized condenser inlet and exit flow regime while measuring condensation heat transfer. They used this data to develop specific heat transfer correlations for stratified and annular flow; however, these correlations are only qualified for round tubes down to 3 mm in diameter.

In the following study we relate condensation heat transfer coefficient measurements to full-length visualization of the flow regimes in a rectangular minichannel tubing condenser that experiences a range of quality, and then develop a predictive correlation that accounts for phase distribution effects. Our focus is on a specific condenser tubing of interest to industry, but the final correlation is intended to have sufficient physical basis to be useful for a range of similar tubes while remaining simple enough to be useful to practicing condenser designers.

2. Test facilities

2.1. Heat exchange loop

The refrigerant loop is depicted in Fig. 1. A variable speed gear pump drives the fluid flow. Adjustment of pump speed and the position of the needle valve control the flow rate. Operating pressure in the loop was stabilized by an accumulator with attached strip heaters. Adjusting the heater power sets the desired accumulator temperature and thus loop operating pressure. The refrigerant flow rate was measured by a mass flow meter. A 2 kW heater was used to heat the subcooled refrigerant such that the condenser inlet state could be controlled. Another 2 kW after-heater provided the ability to superheat, and thus measure the state of, the condensate. These heaters feature a helical flow path to ensure that the heated fluid cannot stratify. A coiled shell-and-tube water-cooled after-condenser returns the refrigerant to a liquid state, with 30–40 K of subcooling.

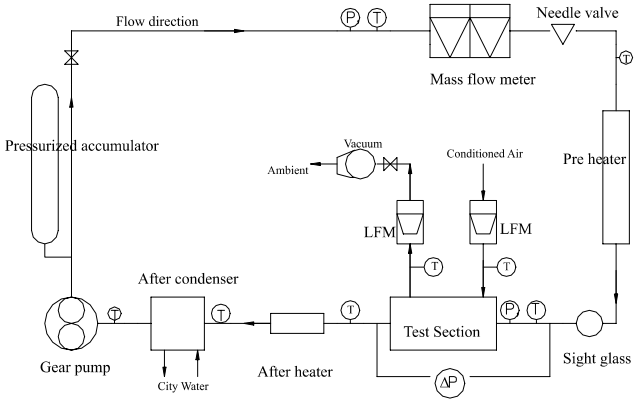

Fig. 1. Schematic of the test facility.

A schematic of the air channel is also shown in Fig. 1. The central component is an air duct fabricated of Plexiglas and insulated with foam boards and fiberglass. Air is drawn through the external fins of the condenser section by a blower controlled by a variable transformer. Two laminar flow elements were used to measure the air flow rates, one at the inlet and the other between the outlet of the air duct and the blower. Each element was connected to a differential pressure manometer. The bulk air temperature was measured by thermocouples placed well upstream and downstream of the test section. A pair of mixing blade flow conditioners were installed to minimize stratification at the downstream thermocouple location.

The 61 cm long air-cooled condenser test section, shown in Fig. 2 is a 10-port tube with a hydraulic diameter of 1.46 mm overall as well as in each individual channel. Louvered fins were brazed to each side of the flat minichannel tubing. This condenser was mounted horizontally in the air channel and connected to the refrigerant loop with a pair of end blocks that provided a gradual transition from the 12.7 mm diameter stainless steel tubes to the minichannel tube. Because the development region is long compared to the tube height, end effects are expected to be minimal. To observe the general state of the refrigerant, sight glasses were installed at the inlet and outlet of the test section. The condenser was instrumented for bulk temperature and pressure at the inlet and outlet. In addition, seven pairs of 40-gauge thermocouples were implanted beneath the edge of the fin roots on the top side of the external leading and trailing tube walls using percussion welding. The fins dominate total heat transfer surface relative to the thin exposed leading and trailing tube edges, so these small thermocouples are expected to accurately represent the

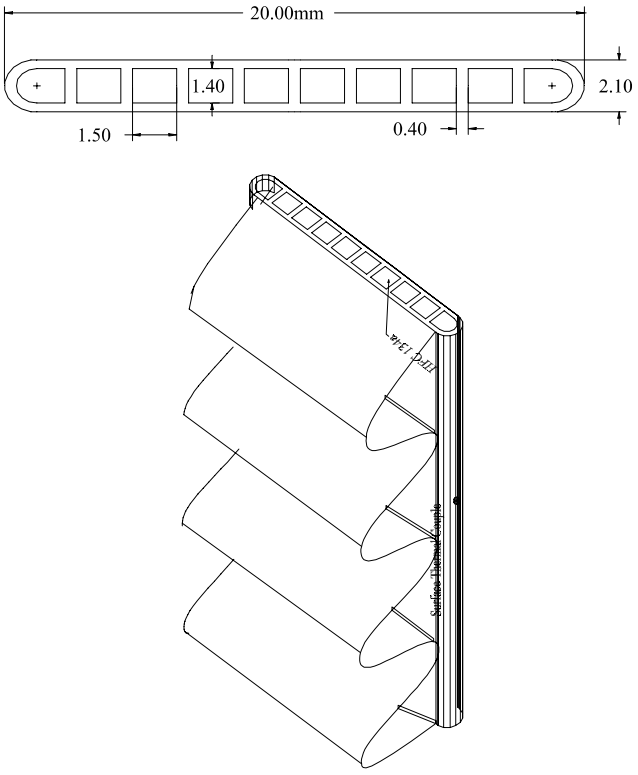

Fig. 2. Condensing test section for heat transfer measurements.

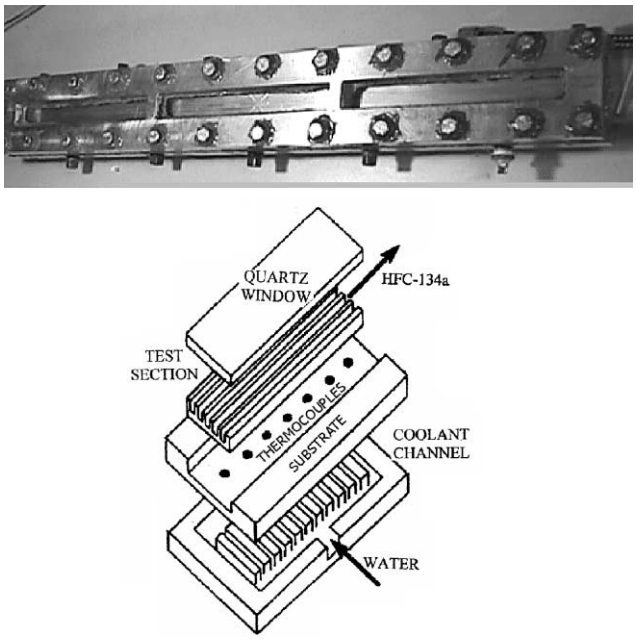

Fig. 3. Condensing test section for flow visualization.

external surface temperatures of the leading and trailing channels. To correlate the local air-side energy balance with these wall measurements, seven thermocouples pairs were installed in the air duct ≈ 3 cm upstream and downstream of the associated condenser wall thermocouples. Pitot-static tubes were also located 3 cm downstream of the corresponding wall thermocouples to measure local relative velocity.

2.2. Flow visualization

A second condenser test section, without fins, was fabricated from a similar minichannel tube specimen with the top surface removed by electrodeposition machining. A glass window was then bonded onto the tube to provide a view of the working fluid. The fully instrumented refrigerant loop from the heat transfer experiment provided fluid at subcooled, saturated, or superheated conditions with flow rates of up to 15 g/s, allowing unambiguous determination of the energy balance and pressure drop across the section.

This test section was mounted in a machined block of aluminum, shown in Fig. 3. Water from the municipal supply was directed over the test section perpendicular to the refrigerant flow to minimize external temperature gradient along the test section. The rate of heat removal was controlled by varying the mass flow rate and by using a heater to control the water temperature. An energy balance on the secondary side was made possible by measuring inlet and outlet temperatures as well as mass flow rate. Note that a relatively low rate of heat transfer is expected through the uncooled window, so external heat transfer from the test section to the environment is not vertically symmetrical as in the heat transfer experiments.

Flow visualization was accomplished by directing light through the window to illuminate the fluid while scattered light from the fluid was recorded with either a video or still camera aimed through the window. A broad region of light was useful in identifying periodic or unsteady flow regimes like slug/plug flow, while annular flow was better characterized by using an angled light sheet to illuminate a cross-section of the fluid at a desired axial location. Polarization of the light and directing illumination at the Brewster angle of either the vapor/window or liquid/window interface allowed good resolution of the fluid and vapor regions. An antireflection coating was also applied to the window to reduce unwanted scatter.

2.3. Data analysis

The basic energy balances for the test are described below. The thermodynamic and transport properties came from three sources: NIST's REFPROP program [16], Dupont [17], and the ASHRAE Handbook of Fundamentals [18]. The heater input power should be equal to the enthalpy increase of the refrigerant plus the heat loss, so

$$\dot{Q}_{\mathrm{h}} = \dot{m}_{\mathrm{r}}(i_{\mathrm{h,o}} - i_{\mathrm{h,i}}) + \dot{Q}_{\mathrm{h,l}}. \tag{1}$$

We can define the heater efficiency, η_h, as

$$\eta_h = \frac{\dot{Q}_h - \dot{Q}_{h,l}}{\dot{Q}_h} = \frac{\dot{m}_r(i_{h,o} - i_{h,i})}{\dot{Q}_h}. \quad (2)$$

This heater efficiency must be evaluated to calculate the condenser inlet refrigerant enthalpy, $i_{r,i}$, and thus the inlet quality, $x_{r,i}$, for two-phase test runs.

$$i_{r,i} = i_{h,i} + \frac{\dot{Q}_h \eta_h}{\dot{m}_r}, \quad (3)$$

$$x_{r,i} = \frac{i_{r,i} - i_l(P_{sat,i})}{i_{fg}(P_{sat,i})}. \quad (4)$$

The energy balance of the test section is given by

$$\dot{Q} = \dot{m}_r(i_{r,i} - i_{r,o}) = \dot{m}_a C_{pa}(T_{a,o} - T_{a,i}) + \dot{Q}_l. \quad (5)$$

From Eq. (5), the local average heat flux across the condenser can be determined from the seven air-side thermocouple measurements if the heat loss to the environment can be estimated. Refrigerant enthalpy and quality can then be determined for each of the seven local sections from the refrigerant inlet conditions and the local average heat fluxes.

Each local averaged section of the test section can be represented as a crossflow heat exchanger. Typically, one would measure the air and refrigerant temperatures, calculate the overall thermal resistance based on a log-mean temperature difference, and separate out the convection coefficient of interest, in our case, that of the refrigerant side. However, for a finned tube, the air-side convection coefficient dominates the overall resistance and makes calculation of refrigerant-side convection from total thermal resistance inaccurate. Instead, the local external tube wall temperature measurements may be applied. The overall resistance between the refrigerant bulk temperature and the external wall surface is

$$R_{tot,rw} = \frac{1}{UA_{rw}} = \frac{1}{[hA]_r} + R_w, \quad (6)$$

where R_w is the wall conduction resistance. If we assume that the external convection coefficient for the fins is relatively constant in the direction of air flow, which is reasonable for the fin pitch-to-length ratio of about 10, then we may apply a crossflow heat exchanger formulation directly to the refrigerant and wall temperatures such that

$$\frac{1}{UA_{rw}} = \frac{F\,LMTD_{rw}}{\dot{Q}}, \quad (7)$$

where

$$LMTD_{rw} = \frac{(T_{ro-} - T_{w,i}) - (T_{ri} - T_{w,o})}{\ln\left(\frac{T_{ro-} - T_{w,i}}{T_{ri} - T_{w,o}}\right)}.$$

Note that F will be unity in condensing flow sections because the fluid temperature will remain constant, while this F-factor must be evaluated from local temperatures given superheated or subcooled flows. Therefore, the local heat transfer coefficient of the refrigerant inside the minichannel tube is given by

$$h_r = \frac{1}{A_r}\left(\frac{F\,LMTD_{rw}}{\dot{Q}} - R_w\right)^{-1}. \quad (8)$$

2.4. Instrumentation and uncertainties

All electrical instrument signals were collected by an Omega signal acquisition system. Type-T special-limit-of-error thermocouples with an uncertainty of ±0.25 °C were used to measure air temperature and condenser wall temperatures. For refrigerant temperature measurements, platinum RTD probes with an uncertainty of ±0.2 °C were submerged into the fluid. All thermocouples and RTDs were calibrated in isothermal ice and boiling water baths using NIST-traceable thermometers with an uncertainty of ±0.05 °C. Calibration curves, which predicted measured temperature to within ±0.25 °C, were developed for each probe.

Strain-gage pressure transducers with ranges of 2 and 3.5 MPa were used to indicate the system pressure and thus verify the fluid saturation temperature during condensation tests. Both transducers were calibrated over their range of applicability with a dead weight tester, giving an uncertainty of ±10.34 kPa. Pressure drop across the test section was obtained from a strain-gage differential pressure transducer with a range from 0 to 69 kPa and an uncertainty estimated as ±0.69 kPa. The power input to the heaters was evaluated from true-RMS voltage and current measurements.

A 38 g/s coriolis mass flow meter was installed to measure the HFC-134a flow rate. An uncertainty of ±0.2% was estimated for the full-scale reading of this flow meter. Laminar flow elements with a 0.02–0.6 m^3/min and 0.3–11 m^3/min range were used to monitor the air volumetric flow rate. These elements have an uncertainty of ±0.25% of the reading. Pitot-static tubes and associated manometers were used to measure the local relative velocity distribution along the tube. These relative measurements, which were deemed accurate to 2%, were biased to agree with the more accurate absolute flow rate from the laminar flow elements.

Propagation of the basic measurement uncertainties given above into the derived parameters needed to reduce the data was evaluated using the method proposed by Moffat [15]. The estimated uncertainty in these

Table 1
Propagated measurement uncertainties

Parameter	Uncertainty [26]
Mass flux = 75 kg/m^2 s	±5%
Mass flux = 750 kg/m^2 s	±0.5%
Heat flux	±5.6%
Quality	±4.2–6.8%
Heat transfer coefficient	±8.2%

experimental parameters is presented in Table 1. It is interesting to note that the uncertainty in heat lost from the air side, Q_l, had little effect on the total uncertainty, which was rather dominated by air-side temperature and flow rate uncertainties.

3. Test results

3.1. Single phase tests

Tests were performed over a wide range of parameters:

- R134a inlet pressure: 18–19.3 bar,
- R134a mass flow rate: 1.66–16.78 g/s,
- R134a mass flux: 75–750 kg/m^2 s,
- R134a inlet temperature: 45–63 °C,
- R134a inlet subcooling: 3–20 °C,
- air inlet temperature: 20–24 °C,
- air flow rate: 0.227–1.019 m^3/min.

Single-phase heat transfer tests provided verification of the experimental apparatus and instrumentation. Because measured temperatures and pressures unambiguously determine the single-phase thermophysical properties, heater efficiencies could be evaluated and the energy balance between the refrigerant and air across the test section could thus be verified. We define the energy balance index, e, as

$$e = \frac{\rho_a Q_a C_{\dot{p}a}(T_{a,o} - T_{a,i})}{\dot{m}_r(i_{r,i} - i_{r,o})}. \quad (9)$$

The resulting values were scattered between 89% and 96%, indicating heat losses across the test section were typically <10%.

Given heater efficiencies, Eqs. (5)–(8) were applied to evaluate the local refrigerant convection coefficient [26]. Because the seven local tube sections were subcooled, refrigerant temperatures were evaluated at the inlet and outlet of the leading and trailing channels of each axial tube section to calculate the F-factor in Eq. (7). Nearly 100 single-phase data were compared to the Gnielinski and Dittus–Boelter correlations as illustrated in Fig. 4. At Reynolds numbers greater than 3000, the data matched within 10% of either correlation. For Reynolds numbers below 1500, the data gave a nearly constant Nusselt number of 7, reasonable for laminar flow in a channel with an aspect ratio of about 10. This comparison thus validates the calculation of convection coefficients.

3.2. Condensation heat transfer tests

Tests were performed over the same range of parameters as the single-phase tests with the following extensions:

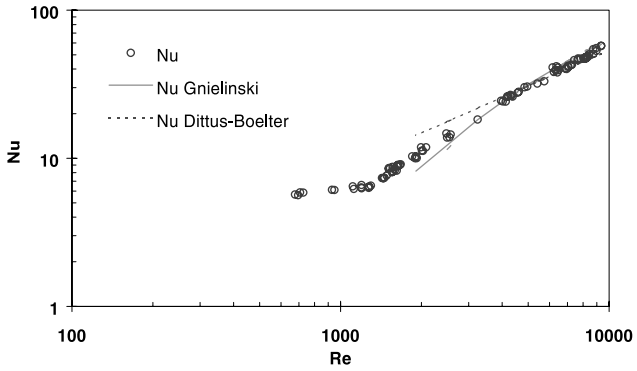

Fig. 4. Nusselt number of the subcooled liquid vs. Reynolds number.

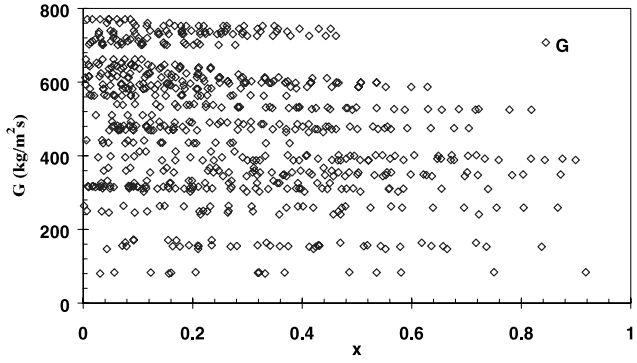

Fig. 5. Mass flux vs. quality for all condensation data points.

- R134a inlet temperature: 61.5–66 °C,
- R134a inlet quality: 0.03–0.94.

Overall, 180 sets of data are presented, representing a wide range of mass flux and quality. Fig. 5 shows the mass flux plotted against the condenser inlet quality for all the collected data. Note that as condensation takes place along the tube the quality decreases from the inlet value, often substantially.

Fig. 6 presents the variation of Nusselt number with mass flux at specific average condenser qualities. The most obvious trend is that Nusselt number becomes more sensitive to mass flux as average quality is increased. We also note that the Nusselt number is least sensitive to quality at the lowest mass fluxes. More interestingly, the trend of heat transfer vs. quality is observed to change as a function of mass flux. This is best seen by evaluating the trend using data at both extremes of mass flux for one value of quality. The two slopes agree given qualities below 0.1 or above 0.4; however, at intermediate values of quality the slope is observed to increase with an apparent break in slope. This break appears to occur at a value of mass flux that decreases as quality increases. Although interesting qualitatively, the data scatter is sufficient to prevent quantitative analysis of this observation.

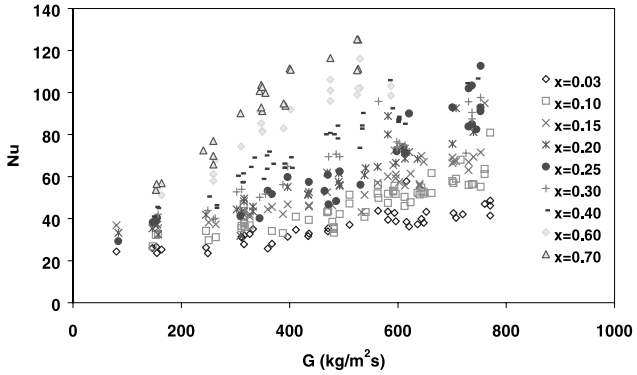

Fig. 6. Condensation Nusselt number vs. mass flux.

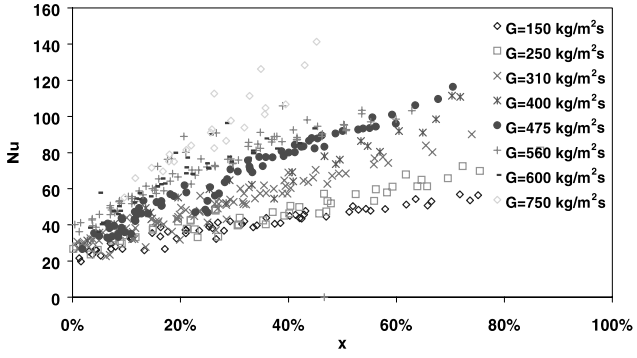

Fig. 7. Condensation Nusselt number vs. quality.

The same general features are seen in Fig. 7, which presents the variation of Nusselt number with quality at specific mass fluxes. As before, Nusselt number becomes more sensitive to quality as mass flux increases and it is least sensitive to mass flux at low qualities. For intermediate values of mass flux the trend of Nusselt number vs. mass flux exhibits less distinct changes in slope. Both increased and decreased slopes are observed as quality is increased.

The behavior observed in these figures can be attributed to the existence of different flow regimes in the condenser. At lower mass fluxes and qualities, a stratified flow regime will prevail over much of the quality range. Heat transfer in a stratified regime is dominated by conduction across the condensate film formed at the top of the tube. The factors that scale heat transfer in this regime are the condensate film thickness and the fraction of the tube circumference over which the film exists; however, the film thickness in a stratified flow regime is not very dependent on mass flux, so neither is the heat transfer. For higher mass fluxes, an annular flow pattern occurs at most qualities. In this flow regime, forced convection at the wall and interface are the major contributors to condensation heat transfer. Velocity drives forced convection, so condensation heat transfer in the high mass flux annular flow regime is strongly quality dependent. Both of these two-phase flow regimes, as well as single-phase fluid, may occur along the condenser tube in any given test.

3.3. Heat transfer data reduction

Several well-known condensation heat transfer correlations were applied to reduce the experiment data. Because of the different condensation mechanisms involved, two categories of correlations were selected. For high mass flux data that falls into the non-stratified and transition regions of the Breber flow regime map presented in Fig. 10, the annular flow correlations of Akers and Rosson [8], Azer et al. [19], Cavallini and Zecchin [20], Shah [21], Chen et al. [22], Dobson and Chato [14], and Traviss et al. [23] were tested. Three types of approaches are encompassed by these annular flow correlations. Akers, Cavallini, Shah, and Dobson based their correlations on two-phase multipliers. Azers and Traviss used boundary layer analysis to develop a correlation, while Chen proposed a shear-based formulation. The film condensation correlations of Chato [24] and Jaster and Kosky [25] were compared with data in the low mass flux stratified flow regime. Only the best predictors, Akers and Jaster et al., are shown in the following section. The remaining comparisons are shown in [26].

The prediction of the Akers correlation for high mass flux tests expected to exhibit primarily annular flow, accounting for 700 of 800 data collected, is shown in Fig. 8. The correlation provides reasonable agreement with the experimental data, with a mean deviation of 15.2%. Most of the data (83.7%) were predicted within ±25%. We see that the correlation tends to overestimate heat transfer at low mass fluxes and underestimate at higher mass fluxes. Overall, Akers correlation predicted the range of microtube flow conditions with fairly satisfactory results, as noted by other researchers, while the other correlations overpredicted heat transfer by a significant margin, particularly at higher qualities.

Fig. 9 displays the prediction of the Jaster and Kosky correlation for the 250 low mass flux data expected to be

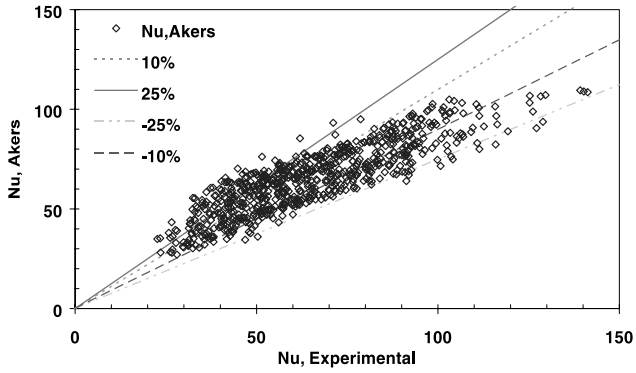

Fig. 8. Comparison of test data with Akers' correlation.

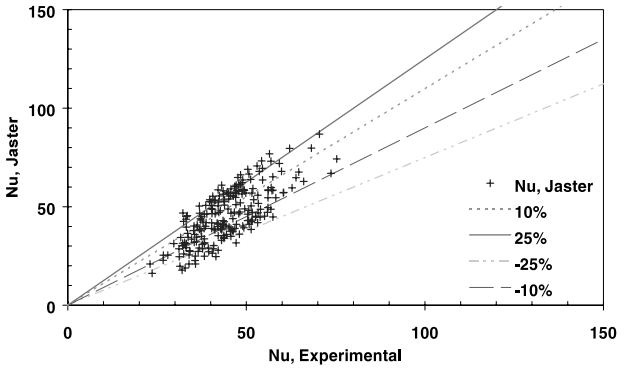

Fig. 9. Comparison of test data with Jaster's correlation.

predominately stratified. Note that there is some overlap in the data points used in the annular and stratified comparison. The transition bands of the Breber flow regime map account for this overlap. By taking the void fraction into consideration, Jaster et al. accounted for the liquid pool depth and quality variation. The prediction was much improved over the Chato correlation and agreed well with the experimental data. The mean deviation between the experimental data and predicted values is 14.9%, and most (80%) are within ±25%.

Note that in the comparisons of both annular and stratified correlations, the data does not reduce entirely linearly. This suggests that the correlations do not scale all of the physics of the experiments.

3.4. Condensation flow regime tests

Various flow patterns were observed during the flow visualization. The quality and mass flux are major factors affecting flow pattern distributions. As the quality was increased from zero at a specific mass flux, slug flow was initially seen, followed by surface waves. As the frequency of the waves increased, a wavy annular pattern was observed. Eventually, a continuous annular liquid film was formed. As mass flux was increased, the flow pattern transitions occurred at lower quality. As a result, the annular regime would occur over most of the quality range at higher mass fluxes. The observed transitions between flow regimes are summarized in Table 2 at various mass fluxes.

Table 2
Transitions of flow regimes

Mass flux, g (kg/m^2 s)	Slug/wavy to wavy/annular, X	Wavy/annular to annular, X
75	0.45	0.88
100	0.38	0.70
150	0.21	0.42
250	0.14	0.30
300	0.12	0.22
350	0.10	0.17

We should note that the relatively low heat removal rate on the observation window may reduce the film thickness on the top of the visualization channel compared to the heat transfer tests.

3.5. Flow regime data reduction

Condensation heat transfer is closely related to flow patterns because different condensation mechanisms occur. Predicting flow regime correctly is thus important to a satisfactory heat transfer correlation. Flow regime maps available from the literature are not known to be valid for millimeter-scale tubing, so we have applied the maps developed by Mandhane et al. [27], Taitel and Dukler [28], Breber et al. [29] and Soliman [30,31], to reduce our data. Only the Breber map and Soliman transitions are discussed below. Other comparisons are given by Wang [26].

The prediction of the Breber map, which scales flow regime on vapor superficial velocity j_v^* and the Martinelli parameter X_{tt}, is shown in Fig. 10. Breber's criteria predicted the wavy and slug flows fairly well; however, the transition from stratified to annular flow was observed to occur at a j_v^* of 0.24 m/s instead of the 0.46 m/s predicted. Given the small cross-section and rectangular geometry of the minichannel tube, surface tension may draw the condensate liquid into the corners, forming an annular liquid film at lower vapor velocity than in the large-diameter round tubes that were the basis of the Breber's map. Note that this trend is opposite of that expected if reduced condensation on the observation window had a significant effect.

The two transitions proposed by Soliman define boundaries between wavy/slug and annular flow, and annular and mist flow, as shown in Fig. 11. Reasonable agreement between the predicted transitions and the results of the visualization was observed. The transition between stratified and annular flow was well predicted at qualities higher than 30%; however, at lower qualities the transition occurred at a smaller mass flux than that predicted by Soliman. This is generally consistent with

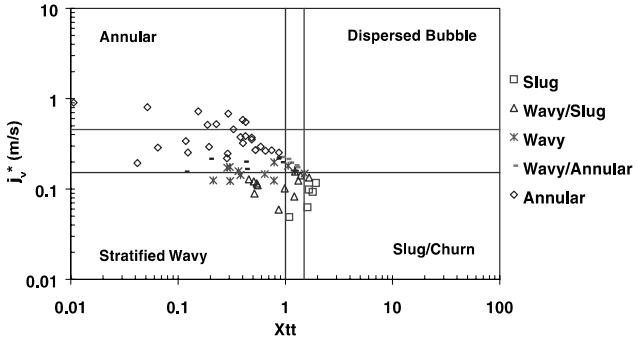

Fig. 10. Flow regime visualization data plotted on a Breber map.

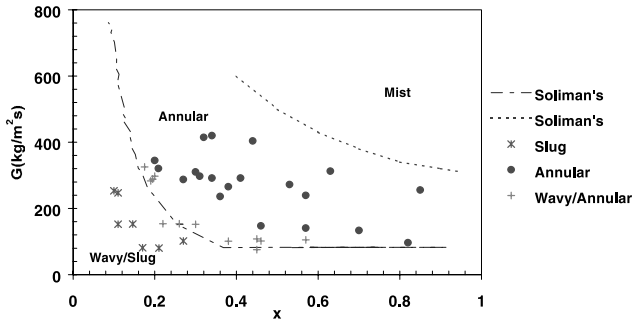

Fig. 11. Flow regime visualization data plotted against Soliman transitions.

the comparison of the data with the Breber model, presumably for the same reason. The transition from annular to mist flow was not observed in the presented data.

4. Condensation heat transfer correlations

To account for the effects of flow regime on condensation heat transfer, we will first develop correlations for the two dominant flow regimes identified by the flow visualization in a manner similar to Dobson and Chato [14]. First is an annular flow heat transfer correlation, which we will base on boundary layer analysis. Next is a stratified flow heat transfer correlation, based on the superposition of filmwise condensation and single-phase forced convection. These correlations are chosen to best represent the physics of the individual flow regimes. Finally, a combined correlation is presented that explicitly accounts for the effects of flow regime transition and is thereby applicable to all of the experimental data.

4.1. Annular flow regime heat transfer correlation

The boundary layer approach developed by Azer et al. [19] and modified by Traviss et al. [23] applies the continuity, momentum, and energy equations to a turbulent boundary layer with the following simplifying assumptions.

- the liquid film is annular and axisymmetric;
- there is no entrainment of liquid in the vapor core;
- both the liquid and vapor are turbulent;
- the universal velocity profile is valid; and
- the liquid film thickness is much smaller than the hydraulic diameter of the tube.

The heat flux within the turbulent annular flow can be defined as follows:

$$\dot{q} = \rho_l C_{pl}(\alpha_l + \varepsilon_h)\frac{\partial T}{\partial y}, \tag{10}$$

where ε_h is a turbulent thermal diffusivity. Also, from the energy equation for steady flow,

$$\frac{\partial}{\partial y}\left(\rho_l C_{pl}(\alpha_l + \varepsilon_h)\frac{\partial T}{\partial y}\right) = 0. \tag{11}$$

This implies that the heat flux is constant in the y-direction and is also equal to the wall heat flux. Eq. (10) can be rearranged and integrated from the wall to the interface in the following form:

$$\int_{T_w}^{T_\delta}\frac{dT}{\dot{q}} = \int_0^{\delta}\frac{dy}{\rho_l C_{pl}(\alpha_l + \varepsilon_h)}. \tag{12}$$

Substituting non-dimensionalized variables, Eq. (12) can be written as

$$\frac{1}{h} = \int_{T_w}^{T_\delta}\frac{dT}{\dot{q}} = \int_0^{\delta^+}\frac{v_l}{\rho_l C_{pl}(\alpha_l + \varepsilon_h)u_\tau}dy^+. \tag{13}$$

Therefore, the heat transfer coefficient, h, can be derived by solving for the unknowns of δ^+, ε_h and τ_w, the main variable represented by u_τ, as functions of y^+. The wall shear stress can be obtained from a friction pressure gradient correlation. The dimensionless film thickness, δ^+, can be found from the continuity of the liquid film. To obtain ε_h, the Reynolds analogy is introduced by assuming a unity value for turbulent Prandtl number.

The liquid-only frictional pressure gradient is defined by

$$\left(\frac{dP}{dz}\right)_l = \tau_w\frac{4}{D_h}. \tag{14}$$

This can be related to the pressure gradient for vapor-only flow by the method of Lockhart and Martinelli [32] as

$$\left(\frac{dP}{dz}\right)_l = \phi_v^2\left(\frac{dP}{dz}\right)_v, \tag{15}$$

where

$$\left(\frac{dP}{dz}\right)_v = \frac{2\left(\frac{4}{\pi}\right)^{2-0.2}0.046\mu_v^{0.2}\left(\dot{m}_v\right)^{2-0.2}}{D_h^{4.8}\rho_v g} = 0.1421\frac{\mu_v^{0.2}\left(\dot{m}_v\right)^{1.8}}{D_h^{4.8}\rho_v g}. \tag{16}$$

So we may therefore find u_τ from the pressure gradient as

$$u_\tau = \left(\frac{g\tau_w}{\rho_l}\right)^{1/2} = 0.152\left(Re_v^{0.9}x^{0.9}\frac{\mu_v}{D_h}\left(\frac{\rho_v}{\rho_l}\right)^{1/2}\right)\phi_v. \tag{17}$$

Substituting Eq. (17) into Eq. (13) and introducing a non-dimensionalized boundary layer temperature,

$$T_\delta^+ = \int_0^{\delta^+} \frac{v_l}{(\alpha_l + \varepsilon_h)}\, dy^+, \tag{18}$$

the Nusselt number can be written as follows:

$$\begin{aligned} Nu &= \frac{hD_h}{k_l} = \frac{\rho_l C_{pl} D_h}{k_l} u_\tau T_\delta^{+^{-1}} \\ &= \frac{\rho_l C_{pl} D_h}{k_l} 0.152 \left(Re_v^{0.9} x^{0.9} \frac{\mu_v}{D_h} \left(\frac{\rho_v}{\rho_l} \right)^{1/2} \right) \phi_v T_\delta^{+^{-1}} \\ &= 0.152\, Pr_l Re_l^{0.9} \frac{1}{X_{tt}} \frac{\phi_v}{T_\delta^+}, \end{aligned} \tag{19}$$

where regression of the experimental data gives the vapor multiplier, ϕ_v,

$$\phi_v = \sqrt{1.376 + 8X_{tt}^{1.655}} \tag{20}$$

and the dimensionless boundary layer temperature

$$T_\delta^+ = 5.4269 \left(\frac{Re_l}{x} \right)^{0.2208}. \tag{21}$$

We note that term ϕ_v/T^+ becomes an empirical two-phase heat transfer multiplier. The regression of this term is substantially different than that found by other researchers, although the two-phase friction multiplier presented recently by Webb [13] may give a similar result with perhaps less physical basis. This result suggests that the annular film in this small rectangular tube has a different configuration than that found in round tubes. The final form of the correlation becomes

$$Nu_{anul} = 0.0274\, Pr_l Re_l^{0.6792} x^{0.2208} \left(\frac{1.376 + 8X_{tt}^{1.655}}{X_{tt}^2} \right)^{0.5}. \tag{22}$$

The prediction of Eq. (22) is compared with the 700 annular flow data in Fig. 12. Agreement with data is much better than that achieved with Akers correlation, with an average deviation of 7.9%. 72.4% of data was predicted within ±10%, and 97% of points were predicted to within ±25%.

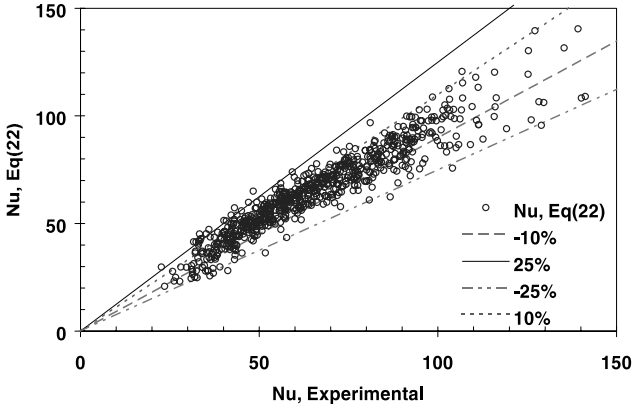

Fig. 12. Comparison of test data with the prediction of Eq. (22).

4.2. Stratified flow regime heat transfer correlation

The heat transfer of the stratified flow results from the superposition of filmwise condensation in the top portion of the tube and forced convection in the bottom liquid pool. For flow with a low mass flux, the heat transfer in the bottom pool is small compared to the filmwise condensation in the top portion of the tube and can be neglected. In addition, the effect of vapor shear on the liquid film is neglected, so the Nusselt theorem becomes applicable as noted by Chato [24] and Jaster and Kosky [25].

As the mass flux increases, neglecting the heat transfer in the bottom liquid pool is no longer reasonable. To account for the additional heat transfer of the bottom pool liquid, a superposition correlation is proposed. The Nusselt number of the stratified flow defined as

$$Nu_{strat} = \alpha Nu_{film} + (1 - \alpha) Nu_{convection}, \tag{23}$$

where the void fraction is used to approximate the fraction of the tube wall where filmwise condensation takes place, while the rest of the interface is occupied by a liquid pool where forced convection dominates. This expression can be simpler than that used by Jaster and Kosky [25] and Dobson and Chato [14] because our tube is rectangular in cross-section. The void fraction is derived from the Zivi [33] correlation.

$$\alpha = \left(1 + \frac{1 - x}{x} \left(\frac{\rho_v}{\rho_l} \right)^{2/3} \right)^{-1}. \tag{24}$$

The first term of Eq. (23) is derived from the Chato [24] correlation for falling film condensation on a horizontal cylinder

$$Nu_{film} = 0.555 \left(\frac{\rho_l (\rho_l - \rho_v) g h_{fg} D_h^3}{k_l \mu_l (T_{sat} - T_w)} \right)^{1/4}, \tag{25}$$

while the second term of Eq. (23) is evaluated by the Dittus-Boelter [34] correlation

$$Nu_{convection} = 0.023 Re_l^{0.8} Pr_l^{0.4}. \tag{26}$$

The prediction of Eq. (23) for 300 stratified flow data is illustrated in Fig. 13. There is considerable improvement over previous results from the literature, with a mean deviation of 6.9%. Over half (63.5%) the data were predicted within ±10%, and less than 1% of data points were not predicted within ±25%. Note that no parameters were adjusted to achieve this improvement.

4.3. Combined regime heat transfer correlation

The correlations developed in the previous sections are specific to particular flow regimes; therefore, there

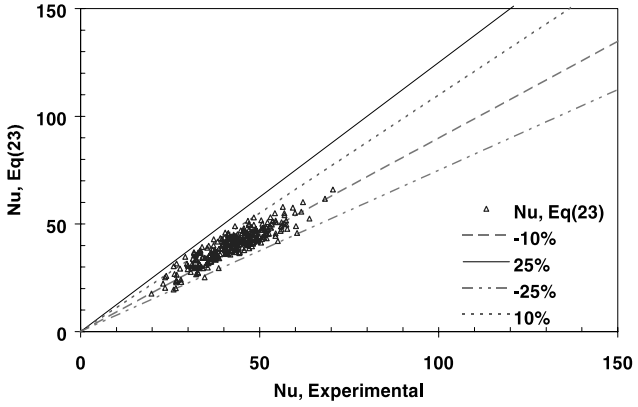

Fig. 13. Comparison of test data with the prediction of Eq. (23).

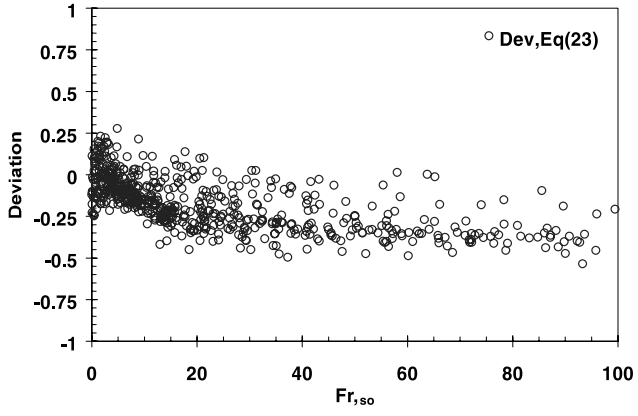

Fig. 14. Deviation of Eq. (23) vs. Froude number.

are limitations for each correlation. Even so, we note that the data expected to represent each regime are not linearly reduced by the respective correlations. To examine their validity, the entire data set was predicted with each correlation. Their deviation was then plotted against the Froude number, Fr_{so} to demonstrate the effect of gravity. For the stratified flow correlation shown in Fig. 14, the average deviation is near zero at low Froude number, but it then trends toward an average deviation of -40% as Fr_{so} is increased above 10. On the other hand, the deviation of the annular correlation, shown in Fig. 15, displays the opposite trend.

The observed deviations suggest that multiple flow regimes may exist in the tube and that a combined stratified-annular correlation, with a transitional factor based on the flow regime transition Froude number, should successfully predict all of the data. The overall heat transfer coefficient, Nu_{all}, can thus be expressed as a combination of the Nusselt numbers, Nu_{anul} from Eq. (22) and Nu_{strat} of Eq. (23), as

$$Nu_{all} = f_{anul}Nu_{anul} + (1 - f_{anul})Nu_{strat}, \quad (27)$$

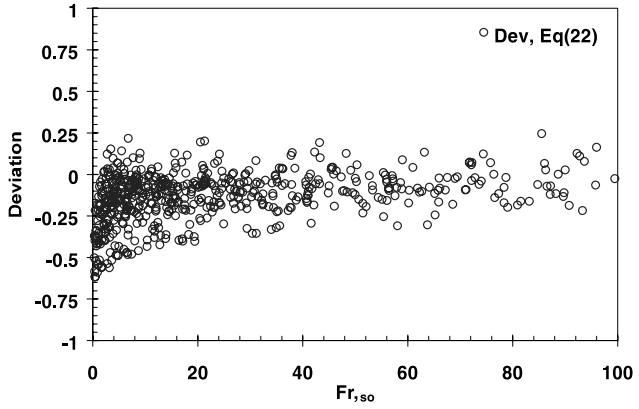

Fig. 15. Deviation of Eq. (22) vs. Froude number.

where f_{anul} is simply the fractional length of minichannel tube experiencing the annular flow regime.

From the flow visualization mapped in Fig. 10, the transition from stratified to annular flow is found to occur at $J_v^* = 0.2$ m/s, which corresponds to a Froude number of 8. This value is somewhat lower than that found by Dobson and Chato [14] for larger round tubes. For a condensing flow of known thermodynamic state and mass flux, the transition Fr_{so} can be represented by a transition quality identified as $x_{trans.}$. Assuming that quality changes linearly along the test section, the fraction of the test section that is in the annular flow regime, f_{anul}, can be expressed as

$$f_{anul} = (x_{in} - x_{trans})/(x_{in} - x_{out}). \quad (28)$$

The prediction of Eq. (27) is plotted for the complete set of data in Fig. 16. The agreement between this correlation and the experimental data is substantially improved, with a mean deviation of 6.1%. Over 79.2% of our data were predicted within $\pm 10\%$. Note that this result is qualitatively and quantitatively better than the results for each individual correlation even when they are compared only to data from the appropriate flow regime.

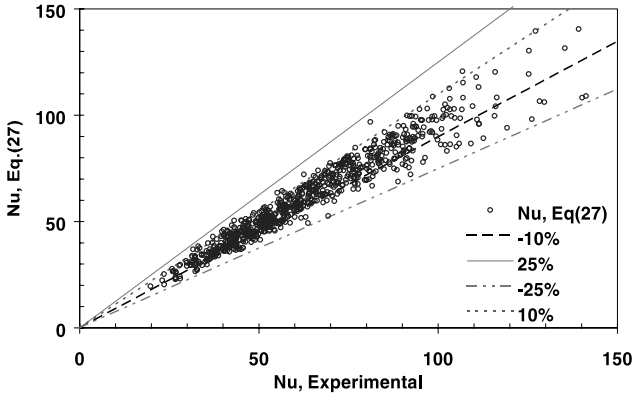

Fig. 16. Comparison of test data with the prediction of Eq. (27).

5. Practical significance

Design of practical condensers currently requires the use of empirical correlations to determine heat transfer coefficients. This paper presents unique heat transfer and flow regime measurements for a rectangular minichannel condenser tube experiencing significant quality change. Comparison of these data to the existing heat transfer correlations and flow regime maps demonstrates that their predictions can be quite inaccurate because of several phase distribution effects specific to this type of tube. The data are reduced to develop a correlation that is based on the physics of each flow regime and which incorporates the measured regime transition point, but is still easy to apply. This correlation is intended for rectangular millimeter-scale tubing condensers in which flow regimes may not be well predicted by current flow regime maps; however, only the values for ϕ_v/T_δ^+ and the regime transition Froude number were developed solely from our data. It is valid in concept for any tube where these quantities are known.

6. Conclusions

In this study we measured condensation heat transfer in millimeter-scale tubes with the complement of full-length flow visualization. Not unexpectedly, we found that the heat transfer coefficient was affected by the flow regime and that the flow regime transitions were not well predicted by existing maps. At low mass flux or low quality, flow stratifies and filmwise Nusselt condensation dominates. Dependence of heat transfer on temperature difference and insensitivity to quality characterize this flow pattern. As mass flux or quality increases, an annular film forms and forced convection prevails. Here, significant dependence on quality and mass flux was observed.

The validity of correlations from the literature was assessed by comparison with the experimental data and shown to be limited. The allegedly incorrectly formulated Akers and Rosson [8] correlation provided reasonable predictions at high mass flux; however, other correlations from the literature overpredicted the measured heat transfer data. Likewise, only the Jaster and Kosky [25] correlation gave an acceptable prediction at low mass fluxes. Although quantitatively acceptable, neither of these correlations reduced the data linearly, suggesting a lack of physical scaling.

To find an improved correlation for our rectangular multi-port tubing, we developed regime-specific correlations with physical bases. Relative to existing correlations, it was necessary to develop a new regression for ϕ_v/T_δ^+ in annular flows. Also, a simple void fraction model was applied to combine filmwise condensation and forced convection heat transfer models for stratified flow in the rectangular tube. Finally, to account for the effect of flow regime transitions over a range of condenser flow conditions, a correlation was developed by weighting the regime-specific correlations with an annular flow length fraction. This fraction was developed from flow visualizations specific to our tube, but public or proprietary regime maps could provide this value for other tubes. As a result, a more accurate prediction of condensation heat transfer coefficient is achieved for minichannel tubing.

7. Recommendations

The data and correlations presented herein are focused on a specific condenser tube of interest to industry. The data is unique, while the derivation of the correlations to predict this data follows a process similar to that used by other researchers. Although the correlations are accurate in predicting our data, it was necessary to evaluate the ϕ_v/T_δ^+ term and the stratified-to-annular transition Froude number from our test data. Similar correlations from several other researchers failed to predict our data accurately, nor will our correlation predict all of their data accurately. To make further progress in development of a correlation that would have general usefulness in condenser tubes small and large, round and rectangular, it will be necessary to scale the effects of surface tension on the formation and the configuration of annular films. Yang and Webb [9] have made progress here in microfinned tubes, but further work is clearly needed.

We are pursuing high-resolution X-ray tomography to determine the steady-state cross-sectional phase distribution along such small tubes during the condensation process. This data could verify models for annular film configuration and flow regime transition without the uncertainties caused by the use of an optical window.

Acknowledgements

The authors would like to recognize Mr. Qun Liu and the Ford Motor Company for their support of this work.

References

[1] C.E. Goodremote, L.A. Guntly, N.F. Costello, Compact air cooled air conditioning condenser, SAE Technical Paper Series, paper number 880445, 1988.

[2] R.A. Struss, J.P. Henkes, L.W. Gabbey, Performance Comparison of HFC-134a and CFC-12 with Various Heat Exchangers in Automotive Air Conditioning Systems, SAE Technical Paper Series, paper number 900598, 1990.

[3] R.A. Struss, L.W. Gabbey, Performance Comparison of HFC-134a and CFC-12 in a Heavy Truck Air Conditioning System, SAE Technical Paper Series paper number 902261, 1990.
[4] A. Sugihara, H.G. Lukas, Performance of Parallel Flow Condensers in Vehicular Applications, SAE Technical Paper Series, paper number 900597, 1990.
[5] R.D. Tait, C.J. Rogers, A.J. Cotton, J.P. Hess, Z.P. Saperstein, Corrosion Resistance of the As Brazed PF Heat Exchanger as Achieved by Alloy Selection, SAE Technical Paper Series, paper number 910594, 1991.
[6] C.Y. Yang, R.L. Webb, Condensation of R-12 in small hydraulic diameter extruded aluminum tubes with and without micro-fins, International Journal of Heat and Mass Transfer 39 (1996) 791–800.
[7] C.Y. Yang, R.L. Webb, Friction pressure drop of R-12 in small hydraulic diameter extruded aluminum tubes with and without micro-fins, International Journal of Heat and Mass Transfer 39 (1996) 801–809.
[8] W.W. Akers, H.F. Rosson, Condensation inside a horizontal tube, Chemical Engineering Progress Symposium Serb 30 (56) (1960) 145–149.
[9] C.Y. Yang, R.L. Webb, A predictive model for condensation in small hydraulic diameter tubes having axial micro-fins, Journal of Heat Transfer 119 (1997) 776–782.
[10] K.W. Moser, R.L. Webb, B. Na, A new equivalent Reynolds number model for condensation in smooth tubes, Journal of Heat Transfer 120 (1998) 410–417.
[11] M.H. Zhang, A new equivalent Reynolds number model for condensation inside smooth and micro-fin tubes, Ph.D. Thesis, Penn State University, University Park, PA, 1997.
[12] L. Friedel, Improved frictional pressure drop correlation for horizontal and vertical two phase pipe flow, Paper E2, European Two Phase Flow Group Meeting, Ispra, Italy, 1979.
[13] R.L. Webb, Prediction of condensation and evaporation in micro-fin and micro-channel tubes, in: Heat Transfer Enhancement of Heat Exchangers, Kluwer Academic Publishers, Dordrecht, 1999, pp. 529–550;
M.K. Dobson, J.C. Chato, Condensation in smooth horizontal tubes, Journal of Heat Transfer 120 (1998) 193–213.
[14] M.K. Dobson, J.C. Chato, Condensation in smooth horizontal tubes, Journal of Heat Transfer 120 (1998) 193–213.
[15] R.J. Moffat, Describing the uncertainties in experimental results, Experimental Thermal and Fluid Science 1 (1988) 3–17.
[16] J. Gallagher, M. McLinden, G. Morrison, M. Huber, REFPROP, National Institute of Standards and Technology. Gaithersburg, MD, 1994.
[17] DuPont, Thermodynamic Properties of HFC-134a (1,1,1,2 Tetrafluoroethane), T-134a-ENG, Document H-4775l-1, E.I. du Pont de Nemours and Co., Wilmington, DE, 1993.
[18] ASHRAE Fundamentals, American Society of Heating, Refrigerating, and AirConditioning Engineers, 1997.
[19] N.Z. Azer, L.V. Abis, H.M. Soliman, Local heat transfer coefficients during annular flow condensation, ASHRAE Transactions 1 (78) (1972) 135–143.
[20] A. Cavallini, R. Zecchin, A dimensionless correlation for heat transfer in forced convective condensation, Proceedings of the Fifth International Heat Transfer Conference, vol. 3, Japan Society of Mechanical Engineers, 1974, pp. 309–313.
[21] M.M. Shah, A general correlation for heat transfer during film condensation inside pipes, International Journal of Heat and Mass Transfer 22 (1979) 547–556.
[22] S.L. Chen, F.M. Gemer, C.L. Tien, General film condensation correlations, Experimental Heat Transfer 1 (1987) 93–107.
[23] D.P. Traviss, W.M. Rohsenow, A.B. Baron, Forced convective condensation in tubes: a heat transfer correlation for condenser design, ASHRAE Transactions 79 (1) (1973) 157–165.
[24] J.C. Chato, Laminar condensation inside horizontal and inclined tubes, ASHRAE Journal 4 (1962) 52–60.
[25] H. Jaster, P.G. Kosky, Condensation in a mixed flow regime, International Journal of Heat and Mass Transfer 19 (1976) 95–99.
[26] W.-William Wang, Condensation and single-phase heat transfer coefficient and flow regime visualization in microchannel tubes for HFC-134a, Ph.D. Thesis, The Ohio State University, Columbus OH, 1999.
[27] J.M. Mandhane, G.A. Gregory, K. Aziz, A flow pattern map for gas-liquid flow in horizontal and inclined pipes, International Journal of Multiphase Flow 1 (1974) 537–553.
[28] Y. Taitel, A.E. Dukler, A model for predicting flow regime transitions in horizontal and hear horizontal gas-liquid flow, American Institute of Chemical Engineering Journal 22 (1) (1976) 47–55.
[29] G. Breber, J.W. Palen, J. Taborek, Prediction of horizontal tubeside condensation of pure components using flow regime criteria, Journal of Heat Transfer 102 (1980) 471–476.
[30] H.M. Soliman, On the annular-to-wavy flow pattern transition during condensation inside horizontal tubes, The Canadian Journal of Chemical Engineering 60 (1982) 475–481.
[31] H.M. Soliman, The mist-annular transition during condensation and its influence on the heat transfer mechanism, International Journal of Multiphase Flow 12 (2) (1986) 277–288.
[32] R.W. Lockhart, R.C. Martinelli, Proposed correlation of data for isothermal, two-phase, two-component flow in pipes, Chemical Engineering Progress 45 (1) (1947) 39–48.
[33] S.M. Zivi, Estimation of steady-state steam void-fraction by means of the principle of minimum entropy production, Journal of Heat Transfer 86 (1964) 247–252.
[34] F.W. Dittus, L.M.K. Boelter, University of California Publications on Engineering 2 (1930) 443.